Archives of Biochemistry and Biophysics 768 (2025) 110391

Contents lists available at ScienceDirect

Archives of Biochemistry and Biophysics

journal homepage: www.elsevier.com/locate/yabbi

Design and synthesis of pyridopyrimidines targeting NEK6 kinase

Paolo Zardi [a,2], Benedetta Righino [b], Davide Pirolli [b], Matteo Gramanzini [b], Alessandro Semeraro [c], Juan José Galano-Frutos [b], Anna Königs [a], Luka Đorđević [a], Michele Maggini [a,d,**], Marianna Buttarelli [e,f], Natalia Cappoli [e,f], Viviana Romano [e,f], Marta De Donato [e,f], Daniela Gallo [e,f,1], Giovanni Scambia [e,f,3], Maria Cristina De Rosa [b,*]

[a] Dipartimento di Scienze Chimiche, Università di Padova, Via Marzolo 1, 35131, Padova, Italy
[b] Istituto di Scienze e Tecnologie Chimiche "Giulio Natta" (SCITEC)-CNR, Roma, L.go F. Vito 1, 00168, Roma, Italy
[c] Dipartimento di Chimica e Tecnologie del Farmaco, Sapienza, Università di Roma, P.le A. Moro 5, 00185, Roma, Italy
[d] Istituto di Chimica della Materia Condensata e di Tecnologie per l'Energia (ICMATE)-CNR, Padova, Corso Stati Uniti 4, 35127, Padova, Italy
[e] Dipartimento Scienze della Salute della Donna, del Bambino e di Sanità Pubblica, Fondazione Policlinico Universitario A. Gemelli, IRCCS, Lgo A. Gemelli 8, 00168, Roma, Italy
[f] Dipartimento Universitario Scienze della Vita e Sanità Pubblica, Sezione di Ginecologia ed Ostetricia, Università Cattolica del Sacro Cuore, Lgo F. Vito 1, 00168, Roma, Italy

A B S T R A C T

We designed a series of pyrido[2,3-*d*]pyrimidine derivatives based on the structure of the NEK6 kinase inhibitor, compound **21** (2-amino-5-phenyl-5,11-dihydro-3H-indeno[2′,1′:5,6]pyrido[2,3-*d*]pyrimidine-4,6-dione), which share the same heterocyclic core. Chemical modifications, aimed at altering the molecular planarity of **21** to enhance water solubility, were guided by receptor-based ligand design and further supported by molecular docking, molecular dynamics simulations, and free energy perturbation calculations. Our results indicate that disrupting the planarity of **21** increases aqueous solubility – nearly doubling it in two cases– while reducing lipophilicity. Among the compounds tested, three showed both improved solubility and NEK6 inhibitory activity exceeding 50 % in single-dose assay.

1. Introduction

NEK6 (Never In Mitosis A (NIMA) related kinase 6) is a serine/threonine kinase involved in mitotic progression [1] whose overexpression has been associated with several cancers, including gastric and breast cancer [2–4]. De Donato et al. also discovered that NEK6 overexpression causes a decrease in sensitivity to cisplatin in the human ovarian carcinoma cell line A2780 [5]. In recent years, the strong association between NEK6 and cancer [6] has driven the development of new therapeutic approaches focused on designing effective inhibitors that target the adenosine triphosphate (ATP) binding pocket of its catalytic domain. NEK6, with 313 residues, is one of the smallest members of the NEK family, consisting solely of the catalytic domain with a short N-terminal extension (residues 20–33). Few structure-based inhibitors, none of them tested for activity in cell lines, had been reported in the literature [7,8] when, in 2018, some of us discovered and patented compounds displaying micromolar efficacy against human ovarian and breast cancer cell lines [9,10]. Using a computer-aided drug design strategy based on the structure of NEK6 generated through homology modeling and knowledge of its known inhibitors, our research team revealed that the substituted 2-oxopyridine derivative **8** and pyrido[2,3-*d*]pyrimidine-4(3*H*)-one derivative **21** exhibited micromolar inhibition in vitro of NEK6 (IC50 = 3.4 μM and 2.6 μM, respectively, Chart 1) [9].

However, compounds **8** and **21** showed limited aqueous solubility, in particular compound **21**, which could hinder their success as drug candidates. A demanding challenge in drug development is to improve aqueous solubility without losing biological activity. To this end, various strategies have been reported, including chemical modification of the molecular structure of the drug candidate itself, exploitation of next-generation drug delivery nanosystems or nanonomatrices, or a combination of both approaches [11,12]. In general, the solubility in water of

* Corresponding author. Istituto di Scienze e Tecnologie Chimiche "Giulio Natta" (SCITEC)-CNR, Roma, L.go F. Vito 1, 00168 Roma, Italy
** Corresponding author. Dipartimento di Scienze Chimiche, Università di Padova, Via Marzolo 1, 35131, Padova, Italy
E-mail address: mariacristina.derosa@cnr.it (M.C. De Rosa).
[1] present address: Department of Toxicology & Pathology Sciences, European Research Biology Center (ERBC), Via Tito Speri 12/14–00071 Pomezia, Italy.
[2] present address: Dipartimento di Scienze Chimiche e Geologiche, Università di Modena e Reggio Emilia, Via G. Campi 103, 41125 Modena, Italy.
[3] This paper is dedicated to the memory of Professor Giovanni Scambia, who passed away on February 20, 2025

https://doi.org/10.1016/j.abb.2025.110391
Received 11 December 2024; Received in revised form 17 February 2025; Accepted 13 March 2025
Available online 14 March 2025

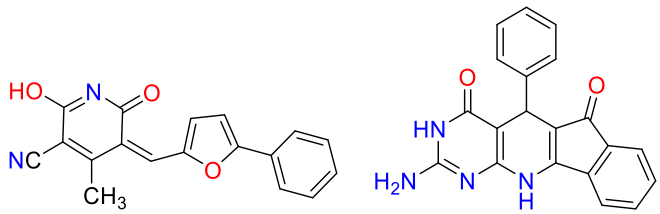

Chart 1. Molecular structures of NEK6 inhibitors **8** and **21**. The numbers are taken from Ref. [9].

small molecules decreases as the lipophilicity (logP) increases. Lipophilicity, on the other hand, can play a positive role as a driving force for the partitioning equilibrium of the drug within the target protein binding site. Thus, finding the appropriate balance is a challenging task, which we tackle here by means of a structural modification of **21**. The introduction of hydrophilic groups into the molecule, although often effective, sometimes interferes with the target protein-drug interaction. Therefore, we considered the alternative strategy to alter the molecular planarity of the condensed cyclic ring system of **21** [13]. We employed a targeted approach combining molecular dynamics (MD) simulations, free energy perturbation (FEP) calculations and logP predictive models to design a series of open-ring derivatives of compound **21**, based on the pyrido[2,3-*d*]pyrimidinone scaffold, achieving improved solubility while preserving biochemical activity. A structure-activity relationship (SAR) study was also conducted on this series, which offers valuable insights to guide future optimization efforts.

2. Results

2.1. Structural modification of compound 21 for ligand design

Compound **21** was synthesized earlier through a three-component reaction, involving benzaldehyde, 2,6-diaminopyrimidine-4(*3H*)-one and indane-1,3-dione in water (Scheme 1) [14].

This synthetic approach was selected to modify the planarity of compound **21**, by replacing the cyclic indane-1,3-dione with acyclic 1,3-diketones, as shown in Scheme 2. Additional molecular diversity can be introduced through the use of various aldehydes to install substituent R_1 on the heterocyclic core structure [15].

2.2. Design of open-ring ligands for NEK6 targeting

Compound **21** was identified through a combined structure- and ligand-based approach, relying on a NEK6 homology model that we developed in 2018. The recent availability of a NEK6 model structure in the AlphaFold database [16,17] prompted us to evaluate this updated structure prior to beginning the optimization of compound **21**. A comparative analysis using protein structure validation tools revealed that our model and the structure generated by AlphaFold2 are of very similar quality (Supplementary Table 1). However, the small α-helix spanning Gly192 and Thr202, which has been observed in the NIMA-related, EGFR, and Src/Hck kinases [18–20] and predicted in NEK6 [21], is only partially formed in the AlphaFold model (Supplementary Fig. 1). As a result, open-ring derivatives of compound **21** were also developed based on our homology model of NEK6, which we specifically selected because it exhibited the α-helical conformation of the T-loop [9]. Structure-based design of **21** open-ring derivatives was carried out using Ligand Designer which after analyzing the structure of the complex formed by NEK6 and **21**, suggested a series of solutions for modifying the structure of the molecule according to Scheme 2.

Fourteen virtual ligands were generated using a bioisosteric replacement protocol and the MPO (multi-parameter optimization) score as the value to be optimized (Supplementary Table 2). Compounds **1–6**, whose Ligand Design score was within 2.5 kcal/mol of that of **21**, were selected (Chart 2).

2.3. Evaluation of the proposed binding modes and affinity predictions

The binding pose and affinity of compounds **21** and **1–6** to NEK6 was estimated *via* molecular docking simulations. Two different docking programs were used, Glide and CDOCKER, which showed similar patterns in binding pose prediction. The RMSD values between predicted Glide and CDOCKER poses, for each docked compound, calculated based on the heavy atom positions, ranged from 0.27 to 1.09 Å (Supplementary Table 2). Compounds **21** and **1–6**, optimized at the NEK6 ATP binding site, shared the same orientation of the pyrido[2,3-*d*]pyrimidinone core structure (Fig. 1). The heavy atoms root mean square deviation (RMSD) between the core moiety of **21** and that of **1–6** was 0.4 Å, 0.4 Å, 0.8 Å, 0.4 Å, 0.5 Å and 0.5 Å, respectively. All compounds are anchored to the NEK6 hinge region through a conserved hydrogen bond network and hydrophobic interactions. Glu123 is hydrogen bonded to nitrogen from NH_2 and NH of the pyrimidine-4-one ring, whose carbonyl oxygen interacts with the NH backbone atom of Ala125. The pyrimidinone ring establishes, for all compounds, π-alkyl interactions with the methyl group of Ala125 and Ala72. Dihydropyridine NH and Asp190 form an additional hydrogen bond that further stabilizes the structure of **21** and **1–6** at the ATP binding site (Fig. 1). The aromatic substituent at position 5 of the pyrido[2,3-*d*]pyrimidinone system forms π-anion interactions with Asp126 in all compounds. In compound **3**, the dihydropyridine ring in this position also forms an additional π-alkyl interaction with Ile51, similarly to compound **5**, which has a furyl moiety (Fig. 1). Replacement of the benzoyl group of **1** and **2** with a methyl ketone in derivatives **3–6** probably releases steric congestion, allowing interactions with Ile51 (Fig. 2).

The stability of compounds **1–6** bound to NEK6 protein was evaluated by MD simulations. The time evolution of NEK6 Cα-RMSD and the variation of ligand-RMSD over time are shown in the Supplementary Fig. 2. The docked poses were relaxed through 10-ns molecular dynamics simulations with the Desmond tool. The RMSD values of NEK6 backbone atoms were identified to be very low (from 0.17 to 0.25 nm) across all the simulations (Supplementary Fig. 2a). Stable RMSD values were also exhibited by the compounds during the simulations, with averages of 0.12 nm, 0.27 nm, 0.34 nm, 0.17 nm, 0.16 nm, 0.08 and

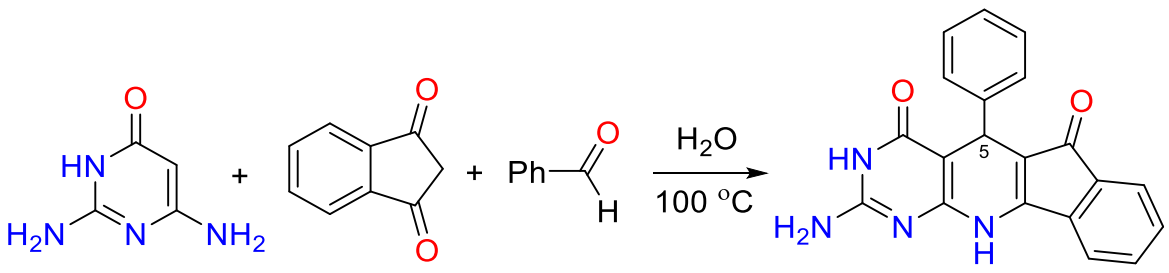

Scheme 1. Synthesis of 2-amino-5-phenyl-5,11-dihydro-3H-indeno[2′,1′:5,6]pyrido[2,3-*d*]pyrimidine-4,6-dione **21** [14].

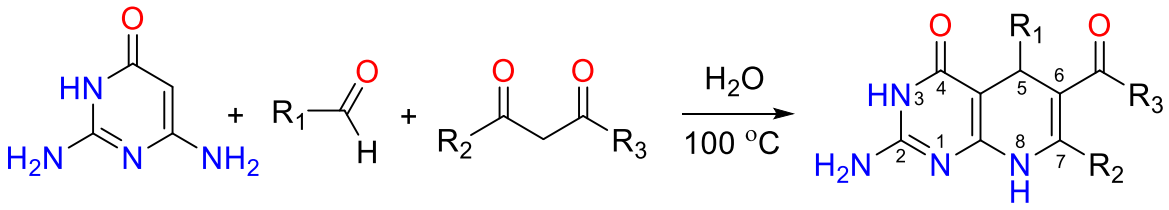

Scheme 2. General procedure for the synthesis of open-ring derivatives of compound **21**.

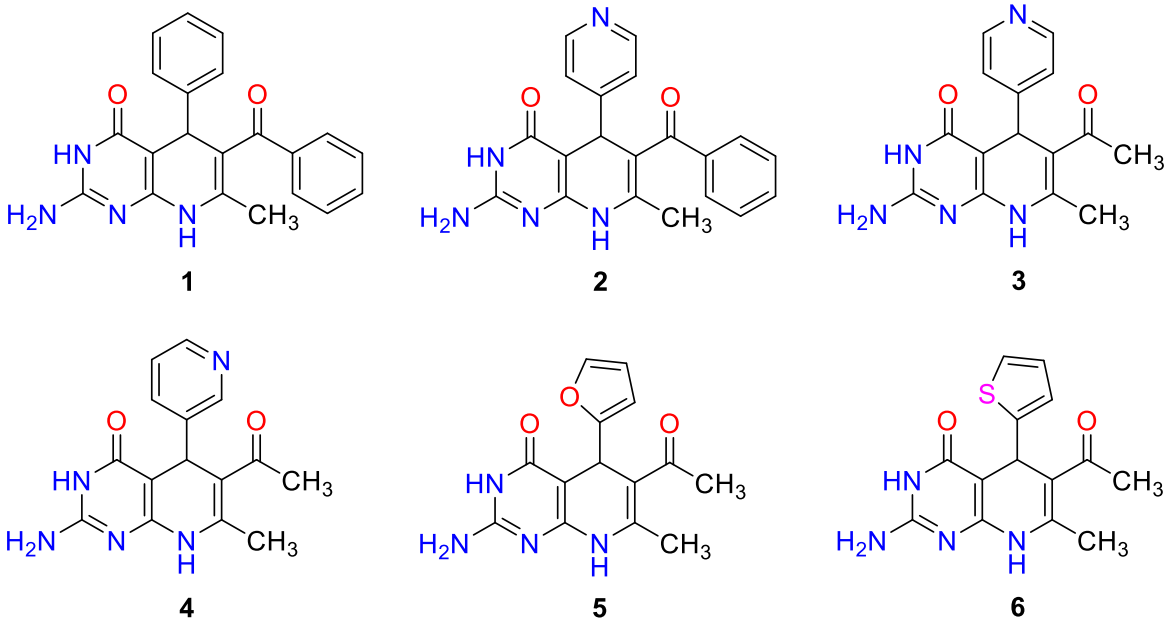

Chart 2. Pyrido[2,3-*d*]pyrimidine-4(3*H*)-one derivatives **1–6** considered in this work.

0.16 nm for compound **21**, and derivatives **1**–**6**, respectively (Supplementary Fig. 2b) which reflects the stability exhibited by the poses along the 10 ns simulated time. 2D interaction diagrams from the MD simulations, showing the frequency of interactions between the ligands and NEK6, are also provided (Supplementary Fig. 3). Free Energy Perturbation (FEP) calculations enable high-confidence predictions of the interaction strength between a ligand and its protein target. FEP uses a series of molecular dynamics simulations in solution to replace one ligand with another and calculate their relative binding free energy difference when bound to NEK6 [22,23]. An increase in binding free energy is indicated by a negative ΔΔG value. Fig. 3 shows the chemical transformations evaluated through FEP calculations for the ligands.

The FEP analysis (Table 1) shows that derivative **3** displays more favorable interactions than compound **21** with the NEK6 ATP binding site ($\Delta\Delta G = -1.324 \pm 0.418$ kcal/mol). For derivatives **2** and **4**, negligible differences in relative ΔG were observed, while more pronounced differences were noted for compounds **5** and **6**. Computed relative free energies indicate that the chemical modifications introduced in compound **3** may improve its binding affinity with NEK6. FEP results further suggest that additional interactions in the open-ring derivatives contribute to enhance binding (Table 1).

2.4. ADME analysis

The evaluation of the pharmacokinetic profile of a molecule is a pivotal aspect in drug discovery and development. The capacity of a small molecule drug to permeate membranes and circulate within the body is strongly associated with its physicochemical properties [24]. ADME predictions for the compounds synthesized and tested in this study were carried out using SwissADME [25]. The main ADME properties provided by this web tool are reported in Table 2. All compounds exhibited lipophilicity values that fell within the range associated to good oral bioavailability ($0 < \log P < 3$) [22,26,27] and that are indicative of good permeability, solubility, and low *in vivo* toxicity [23,28].

Compounds **21** and **1–6** are predicted to have high gastrointestinal (GI) absorption but not blood-brain barrier (BBB) permeability. Interestingly, unlike compounds **21** and **1–2**, compounds **3–6** are not a P-glycoprotein (P-gp) substrate. This suggests that compounds **3–6** could be less susceptible to resistance by this efflux protein and therefore could have better bioavailability and greater ability to reach target sites within the organism [29,30]. All compounds satisfied Lipinski's rule of five [26] and the Abbot bioavailability score (ABS), which predicts the probability of a compound to have >10 % oral bioavailability in a rat model, was 0.55, indicating good absorption after oral administration [31,32]. To exclude the tendency to unspecific biomolecular interactions of the compounds studied, the PAINS (Pan Assay Interference Compounds) score was calculated [33] and did not identify alerts (Table 2).

2.5. Synthesis

The reaction of 2,6-diaminopyrimid-4(3*H*)-one with the proper aldehyde and acyclic 1,3-diketone in water at 100 °C overnight gives, in a single step, the derivatives **1–6** considered in this work, where the ring-fused indeno moiety of **21** is replaced by two different substituents (Chart 2). After filtration of the crude precipitate from the reaction

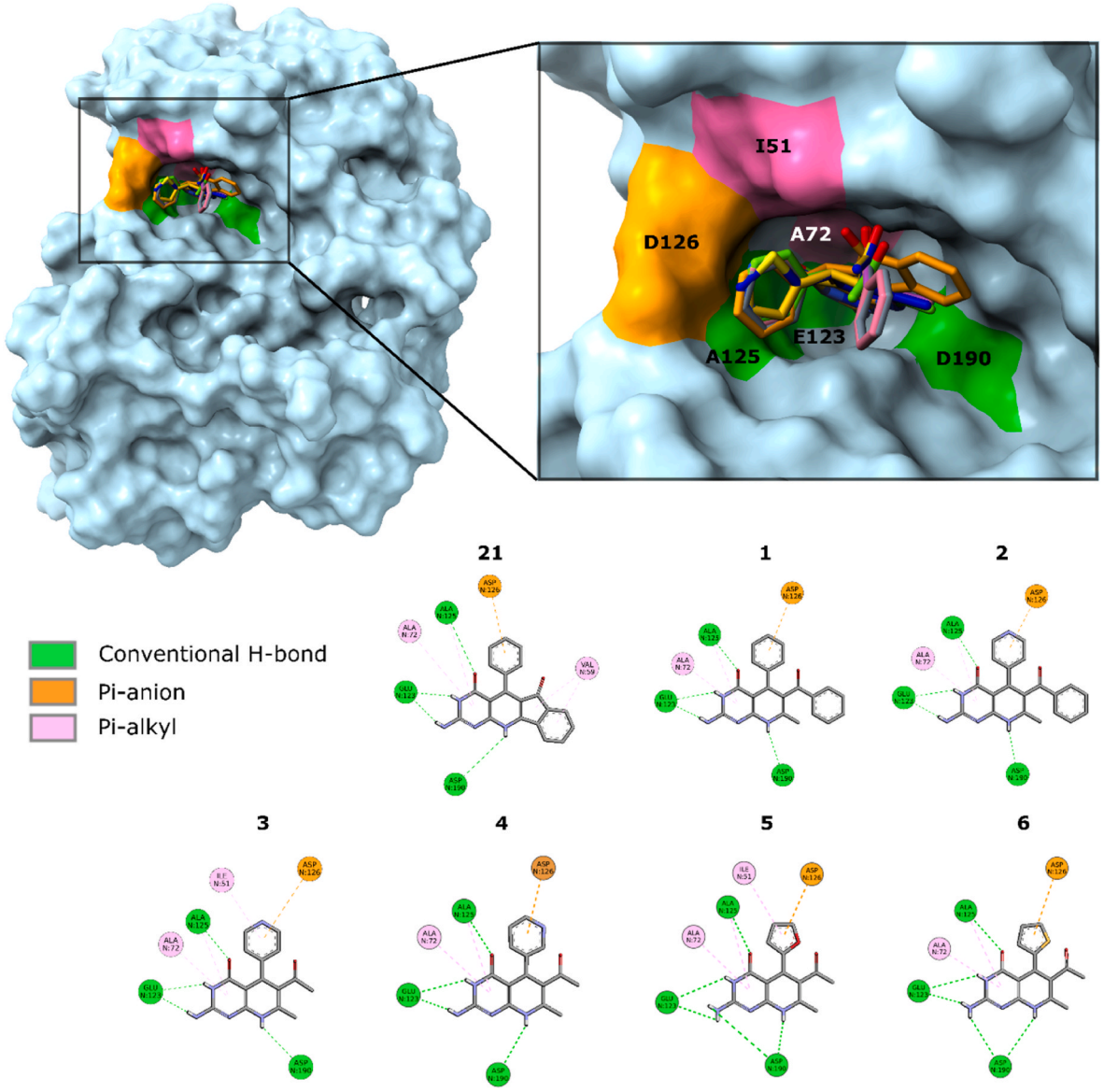

Fig. 1. Molecular interactions of compounds **21** and **1–6** with NEK6. Top: Solid surface of NEK6 showing protein ligand complexes with zoom view on the key interacting residues. Compounds **21** and **1–6** are displayed in sticks without hydrogen atoms. Bottom: 2D protein-ligand interaction diagrams of compounds **21** and **1–6**, showing the interacting amino acid residues within the NEK6 binding pocket. The 2D diagrams were generated with BIOVIA Discovery Studio 2022 showing only hydrogen atoms involved in non-bonding interactions.

mixture, derivative **1** was purified by flash column chromatography (SiO_2), giving a pale-yellow solid in an isolated yield of 18 %. The very low solubility in common organic solvents and high polarity of **1** made its chromatographic purification quite challenging and this is probably the reason for the low yield observed. Derivatives **2–6** were instead purified by washing the crude filtrate with hot acetone and isolated, as pale-yellow solids, in 66 %, 74 %, 49 %, 59 % and 84 % yields, respectively. The six products were characterized by ^{1}H NMR, ^{13}C NMR, IR, UV-is, and high-resolution mass spectrometry. The determination of the melting point for all six compounds gave unsatisfactory results because they undergo decomposition, before melting, at T > 250 °C. The ^{1}H NMR in DMSO-d_6 of **1–6** (Supplementary Fig. 4-9) shows, for nitrogen protons, a broad singlet at around 6.3 ppm (-NH_2) and two singlets at around 9.2 ppm and 10.4 ppm (–NH–), respectively. The proton at position 5 of the dihydropyridine ring is a singlet in the range 4.9–5.2 ppm. The characteristic four protons of the 4-pyridyl ring in **2** and **3** appear as two doublets at around 7.2 ppm and 8.4 ppm, respectively. The four protons of the 3-pyridyl ring in **4** resonate at around 7.2, 7.5, 8.3 and 8.45 ppm, whereas the three protons of the 2-furanyl and 2-thiophenyl rings in **5** and **6** resonate at around 5.8, 6.2 and 7.4 ppm and 6.7, 6.8 and 7.1 ppm, respectively. The use of nonsymmetric benzoylacetone (Scheme 2) can give, in principle, two regioisomers, **1/1r** and **2/2r** (Chart 3). However, only regioisomers **1** and **2** were isolated. Their structure was uniquely assigned by ^{1}H–^{13}C HMBC NMR spectroscopy, where a clear correlation was observed between the ^{13}C resonance of ketone carbonyl and those due to the *ortho* protons of the benzene ring in the ^{1}H NMR spectrum. This indicates that **1** and **2** contain a benzoyl moiety (Supplementary Fig. 10-11).

The observed selectivity comes from the ring closure step, illustrated graphically in Chart 3b, which involves the nucleophilic attack of a primary amino group of the 2,6-diaminopyrimidinone moiety in one of the two carbonyl groups [14,34]. The reduced reactivity of aryl ketones to nucleophilic attack, compared to alkyl ketones [35–37], explains the selectivity for the structure of derivatives **1** and **2**. The solubility of compounds **1–6** was determined in a H_2O/DMSO 99:1 mixture using the calibrated additions method (see materials and methods). This solvent

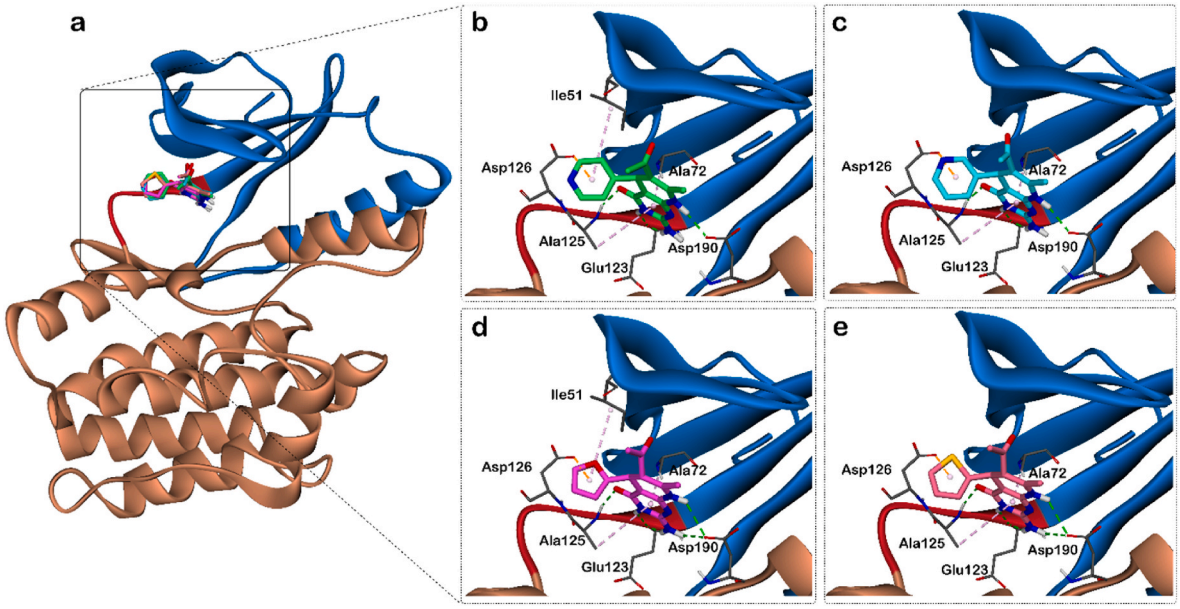

Fig. 2. Three-dimensional representation of the predicted binding mode of compounds **3–6**. (a) Overlapped predicted poses of compounds **3–6** within the NEK6 binding pocket. The N-lobe domain of NEK6 is colored blue, the C-lobe khaki, and the hinge region red salmon. (b–e) Zoomed-in views of the complexes with compounds **3–6**, respectively, showing the key interacting residues in stick representation, color-coded by atom type. Interactions between the compounds and the binding site are depicted as follows: Interactions between the compounds and the binding site are depicted as follows: hydrogen bonds in green, π-anion interactions in orange, and π-alkyl interactions in purple. The binding modes were generated using the Glide docking tool, whereas the protein-ligand interactions were evaluated using BIOVIA Discovery Studio 2022. (For interpretation of the references to color in this figure legend, the reader is referred to the Web version of this article.)

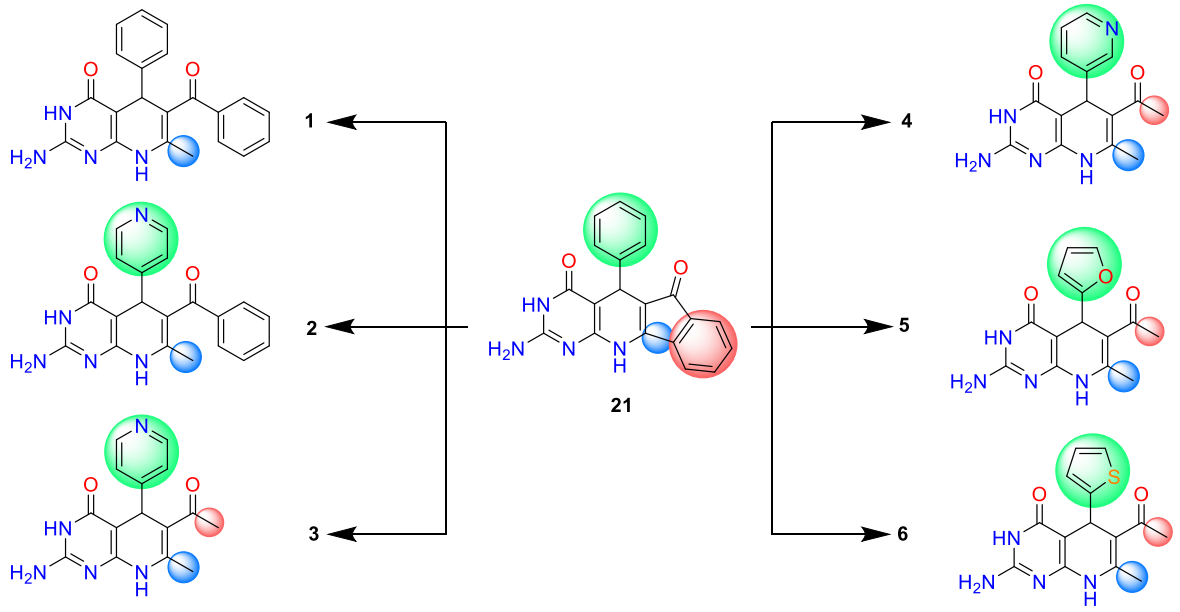

Fig. 3. Modifications of substituents in free energy perturbation calculations. Highlighted with green, blue and orange spheres appear the regions where modifications are introduced. (For interpretation of the references to color in this figure legend, the reader is referred to the Web version of this article.)

mixture was chosen because it is used for the biochemical NEK6 inhibition test (*vide infra*). At 25 °C the measured solubility for **1** is 150 μg/ml, for **2** is 340 μg/ml for **3** is 500 μg/ml, for **4** is 640 μg/ml, for **5** is 500 μg/ml and for **6** is 134 μg/ml. For comparison, the solubility of **21** is 280 μg/ml, measured by us under the same conditions. Derivatives **1** and **6** are less soluble than **21**. It is interesting to note that derivative **1** shows a distinctive high resolution mass spectrum. Unlike compounds **2–6** and **21**, the ESI + spectrum of **1**, recorded in water or methanol, shows, in addition to its expected monoisotopic mass shown in Supplementary Fig. 12, a series of seven more clusters at *m/z* values that correspond to supramolecular oligomeric species in which up to 11 units of compound **1** aggregate (Fig. 4). NMR, HRMS, IR and UV–vis spectra of derivatives 1–6 are reported in Supplementary Figs. 12–24.

The structure of **1** (Fig. 4) can be considered amphiphilic, where the two hydrophobic aromatic rings are almost orthogonal to the more hydrophilic pyrido[2,3-*d*]pyrimidinone core. Therefore, it is reasonable to assume that **1** can self-associate in a polar solvent to form a variety of morphologies that high resolution mass spectrometry detects at different *m/z* values [38]. Although this finding refers to supramolecular dynamics that take place inside a mass spectrometer, it reflects the low

Table 1
FEP calculations on derivatives **1–6** in the NEK6 ATP binding site, relative to inhibitor **21**.

FEP transformation	ΔΔG (kcal/mol)
21 → 1	0.05 ± 0.94
21 → 2	−0.23 ± 0.23
21 → 3	−1.32 ± 0.42
21 → 4	−0.16 ± 0.95
21 → 5	−0.82 ± 0.34
21 → 6	−0.74 ± 0.50

solubility of **1** and its potential tendency to aggregate in polar environments, that was further evidenced by TEM analysis (Supplementary Fig. 25). The amphiphilic characteristics of compound **1** are mitigated by the heteroaromatic ring, which replaces the benzene ring in compounds **2–6**, and by a methyl ketone, which replaces the benzoyl moiety in compounds **3–6**. However, derivative **6** turned out to be even less soluble than compound **1**. This is possibly due to the sulfur atom in thiophene, which is less electronegative than oxygen or nitrogen, making thiophene more hydrophobic compared to other heterocycles like furan or pyridine. This hydrophobicity is most likely the reason why derivative **6** is the least soluble in the H_2O/DMSO 99:1 solvent mixture.

2.6. Biochemical kinase assay

The NEK6 inhibitory activity of derivatives **1–6** was tested at a single dose of 30 μM to assess their relative inhibitory potency compared to compound **21**. Fig. 5 shows the percent of NEK6 activity retained after treatment with **21** and derivatives **1–6**. All compounds, except compound **2**, exhibited more than 50 % inhibition of NEK6 kinase activity. Notably, compounds **3**–**6** showed potency comparable to or greater than that of the reference compound **21**, indicating that the opening of the indenone ring system, along with the modifications depicted in Fig. 3, is well-tolerated. The NEK6 inhibitory potency observed in the compound series **1–6** aligns with the FEP calculations, highlighting the effectiveness of the receptor-based design approach employed in this study.

2.7. SAR/QSAR analysis

SAR and QSAR are widely used computational tools in medicinal chemistry, analyzing features like solubility, acidity, and polarity as molecular descriptors to identify key determinants for tasks such as toxicity, drug-likeness, or enzyme binding [39]. These insights guide the improvement of properties or activities in drug development projects [40–42]. In this study, a SAR analysis was performed using experimentally measured activity and properties (e.g., NEK6 % inhibition and solubility, Supplementary Table 3). A set of 94 interpretable molecular descriptors (MoDs) was selected, filtered, and used to explore structure-activity and structure-property relationships. Supplementary Table 4 contains the 37 filtered MoDs along with their individual squared Pearson correlation coefficient (R^2) in relation to both measured properties: NEK6 % inhibition and compounds' solubility. An analysis of these statistics reveals that certain descriptors, such as spherosity (SPH)—an anisometry measure quantifying the sphericity of a compound's shape [43]—and total surface area (SAtot), show a strong

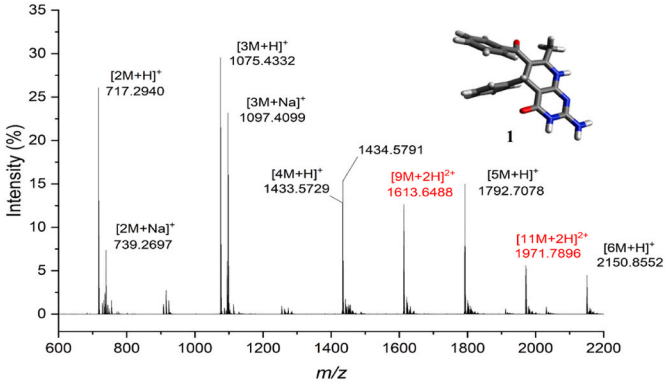

Fig. 4. HRMS (ESI+) of pyrido[2,3-*d*]pyrimidine-4(3*H*)-one derivative **1** ($C_{21}H_{18}N_4O_2$) in water. Calc. [9 M+2H]$^{2+}$ 1613.6537; calc. [11 M+2H]$^{2+}$ 1971.7966.

Table 2
Selected drug-likeness and pharmacokinetic properties of compounds **21** and **1–6**.

Cpd	Lipophilicity	Pharmacokinetics			Drug-likeness			MedChem
	logP	BBB permeant	GI abs	P-gp substrate	Lipinski	Veber	Bio availability score	PAINS
21	2.01	No	High	Yes	Yes no violation	Yes	0.55	no alert
1	2.47	No	High	Yes	Yes no violation	Yes	0.55	no alert
2	1.74	No	High	Yes	Yes no violation	Yes	0.55	no alert
3	0.67	No	High	No	Yes no violation	Yes	0.55	no alert
4	1.08	No	High	No	Yes no violation	Yes	0.55	no alert
5	1.34	No	High	No	Yes no violation	Yes	0.55	no alert
6	1.38	No	High	No	Yes no violation	Yes	0.55	no alert

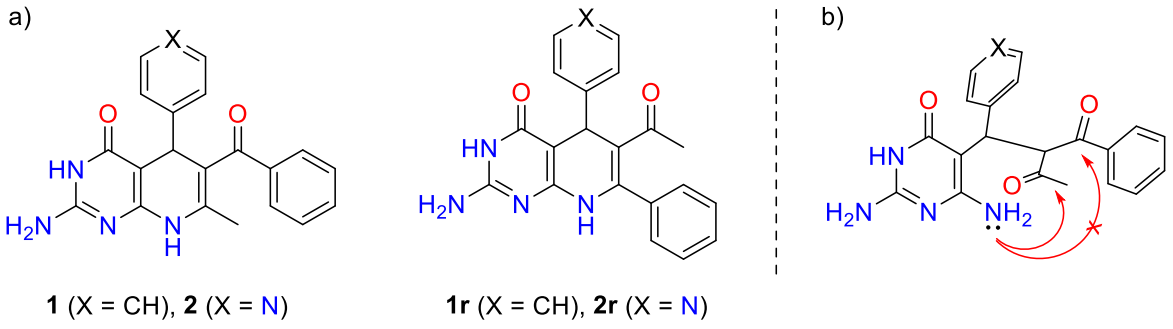

Chart 3. a) Representation of the two possible regioisomers that may form when benzoylacetone is used as 1,3-diketone. b) Proposed reaction intermediate showing the ring closure selectivity.

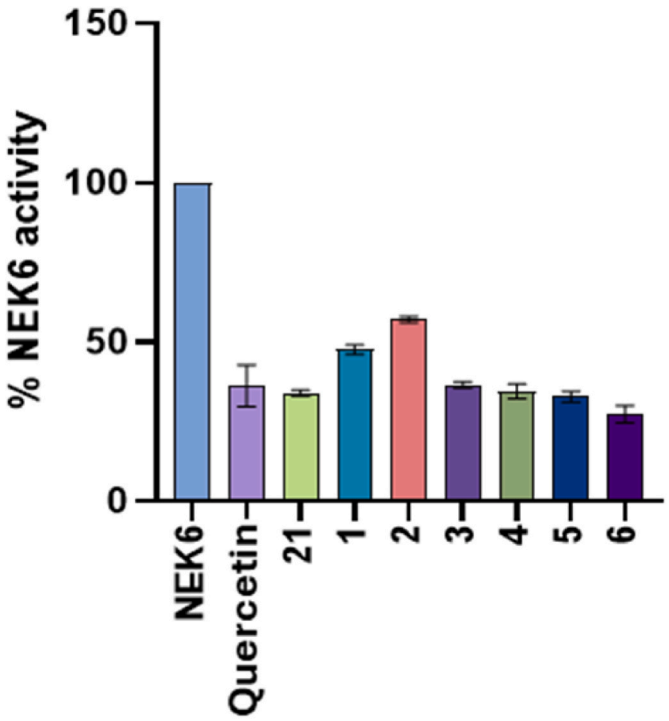

Fig. 5. Bar graph showing the percentage of NEK6 activity retained (mean ± SEM, n = 3) after the addition of each compound at a single dose of 30 μM, using the LANCE Ultra TR-FRET kinase assay.

correlation ($R^2 > 0.8$) with NEK6 inhibitory activity. The coefficient signs of descriptors SPH (positive) and SAtot (negative) in correlation with NEK6 inhibition activity (see footnotes in Supplementary Table 4) indicate that compounds with a more spherical shape and simultaneously a smaller surface area will tend to enhance NEK6 inhibition. Including these two MoDs in a predictive model would be impractical due to their strong correlation (−0.95), which could result in overfitting and unstable coefficients. In contrast, the best-correlated MoDs (N% and ALOGP) showed much lower individual correlations with the solubility endpoint (0.62 and 0.57, respectively, Supplementary Table 4). The positive correlation of N% (Supplementary Table 4) suggests that the addition of more nitrogen atoms in proper positions could favour the solubility of these compounds. ALOGP, the calculated Ghose-Crippen octanol-water partition coefficient, exhibits a negative correlation with solubility as expected. Additionally, a strong negative correlation (−0.92) between N% and ALOGP prevents their combined use in a QSAR predictive model, particularly given the limitations of our dataset. No single MoD shows strong correlations with both endpoints, likely because solubility and binding to biological macromolecules often rely on opposing physical properties due to the hydrophobic nature of macromolecular interacting surfaces. This underscores the difficulty of optimizing multiple drug-like properties simultaneously. No multi-descriptor models outperformed the single-MoD model incorporating SPH for the NEK6 inhibition endpoint (Supplementary Table 4). Instead, a better multi-descriptor model was identified for the solubility endpoint (see Eq. (1) and Table 3), providing valuable insights in order to enhance this property within the derivative series.

$$\text{Solubility} = 46.51(\pm 31.65)\text{*SPH} + 146.15(\pm 26.29)\text{*N\%} + 113.20(\pm 28.65)\text{*AROM} + 363.43(\pm 49.02) \quad \text{Eq. 1}$$

3. Conclusions

In this study, we designed, synthesized, and evaluated a series of pyrido[2,3-*d*]pyrimidine derivatives based on the previously identified compound **21**. The primary objective was to enhance solubility while maintaining or potentially improving NEK6 kinase inhibitory activity. To achieve this, we incorporated an acyclic ketone during the synthesis to disrupt the planarity of compound **21** and applied structure-based molecular design strategies, ultimately leading to the development of derivatives **1**–**6**. Among these, compounds **2**–**5** demonstrated improved solubility in the 99:1H_2O/DMSO mixture used for the biochemical kinase assay. The reduced solubility of compound **1** was likely due to its tendency to aggregate in polar environments, whereas the thiophene ring in compound **6** contributed to a stronger hydrophobic character compared to furan or pyridine substitutions. The calculated lipophilicity values (logP) revealed that, with the exception of compound **1**, all derivatives were less lipophilic than **21**. This finding underscores the importance of heterocyclic substitutions in designing soluble inhibitors. The planarity-disruption strategy clearly aligns with the gain in a more spherical shape (SPH) of the compounds, identified as a key feature through the SAR/QSAR analysis to enhance the druggability properties of this compound series. The analysis also revealed that chemical modifications leading to combined increases in SPH, aromaticity index (AROM), and nitrogen atom content (%) contributed to enhancing the compounds' solubility. FEP simulations indicated that the reduced lipophilicity of these derivatives did not compromise their binding affinity. Molecular modeling and FEP calculations further revealed that the aromatic heterocyclic substituent at position 5 of the dihydropyridine ring interacts effectively with the NEK6 active site, supporting the rationale for the observed activity. Additionally, the calculated pharmacokinetic profiles of all compounds were favorable. Notably, compounds **3**–**6** exhibited moderate NEK6 inhibitory activity, with inhibition percentages comparable to compound **21** and, in the case of compound **6**, even superior activity. FEP simulations suggest that compound **3** could be a more potent inhibitor than compound **21**. However, its modest activity is likely attributed to unmodeled limiting factors. Overall, the experimental data indicate that the ring-opening strategy enhances the solubility of the derivatives while preserving their NEK6 activity. Further modifications to the pyrido[2,3-*d*]pyrimidinone core are currently in progress to explore and validate the therapeutic potential of these compounds.

Table 3
Statistics of the multi-descriptor QSAR model obtained for compounds' solubility.

Model parameter	Value
R^2	0.94
p-value (model)[a]	0.02
p-value (SPH)[b]	0.02
p-value (N%)[b]	0.01
p-value (AROM)[b]	0.03
p-value (constant)[b]	0.00
Cond. Number[c]	1.78
Max residual[d]	−77.79

[a] From a Fisher's statistical test.
[b] From a *t* statistical test.
[c] The condition number [44] is a crucial metric that assesses the sensitivity of the regression coefficients to perturbations in the data. Generally, a condition number less than 10 indicates a well-conditioned model, suggesting stable and reliable coefficient estimates with minimal numerical errors.
[d] Maximum difference between predicted and measured solubility across all compounds.

4. Materials and methods

4.1. Receptor-based modeling

Molecular modelling was carried out using the Maestro software package of the Schrödinger suite of programs (Schrödinger Release

2022–1, Schrödinger, LLC, New York, NY, 2022). Comparative assessment of the NEK6 homology modeling previously generated [9] and the structure of NEK6 in AlphaFold database [16] was carried out. The analysis involved the following protein structure validation servers: ERRAT [45], PROCHECK [46], ProSA [47] and MolProbity [48]. A summary of the results is provided in Supplementary Table 1. The comparison led to the selection of the NEK6 homology modeling [9] (see the **Results** section). Accordingly, the pose predicted by molecular docking for compound **21** in complex with NEK6 [9] was used as the starting point to optimize its druggability profile. Using compound **21** in complex with NEK6 in the pose predicted by molecular docking as starting point [9] we used the Ligand Designer tool to manually modifying the structure of the ligand and build the molecular structures of compounds **1**–**6** while maintaining the main interactions of **21** with the ATP site of NEK6. The protein was prepared using the protein preparation wizard, which checks the structure for errors or missing atoms and fix them, assigns hydrogens and charge states of ionizable groups at pH 7.4, assigns the force field parameters to the system's atoms and optimizes the structure by energy minimization. OPLS4 force field [49] was used to represent all compounds and protein. In Ligand Designer, after each modification, an evaluation of the parameters used to assess drug-likeness (LogP, molecular weight, polar surface area, and the number of hydrogen bond donors/acceptors) was performed for every derivative. Additionally, in-situ minimization was carried out to better accommodate the new ligand within the ATP site. Molecular docking was performed to position ligands **21** and **1–6** into NEK6 binding site. The docking studies were carried out with two programs, Glide with XP precision (Schrodinger) and CDOCKER (BIOVIA) which use different searching methods and scoring functions and are therefore appropriate for comparison purposes.

4.2. Molecular dynamics simulations

All-atom molecular dynamics simulations of predicted complexes were performed using the Desmond software package (Schrödinger Release 2024–1: Desmond Molecular Dynamics System, D. E. Shaw Research, New York, NY, 2024) as implemented in Maestro. Each complex between NEK6 and the docked ligand was embedded in a cubic box, with its faces placed at a minimum distance of 10 Å from the complex's atoms and solvated with SPCE water models. The solvated systems were then neutralized using Cl^-ions, and a concentration of 0.15 M NaCl was simulated by adding additional $Na^+$and Cl^-ions. The Particle-Mesh Ewald method was employed to represent the long-range electrostatic interactions [50]. A cut-off radius of 9.0 Å was applied for short-range van der Waals and Coulomb interactions. Each solvated system was first minimized and then equilibrated using the default relaxation protocol of Desmond. All equilibrated systems were then submitted to a production run at constant pressure and temperature (NPT) for 10 ns. The temperature of 300 K and the pressure of 1 atm were maintained by the Nosé-Hoover chain thermostat and Martyna-Tobias-Klein barostat methods, respectively [51]. Trajectories from the MD simulations were analyzed using the "Simulation Interaction Diagram" tool as implemented in Maestro.

4.3. FEP calculations

All steps of free energy perturbation (FEP) calculations were carried out using Discovery Studio 2022 (BIOVIA, Dassault Systèmes, Discovery Studio, Discovery Studio 2022, San Diego: Dassault Systèmes, 2022). The predicted binding mode of **21** [9] was used as template and **1–6** ligands, were aligned in the binding site. Each solvated ligand and complex system was prepared for FEP calculation using the "Generate Ligand Pairs protocol" and simulated for 3 ns using 14 λ windows (0.0, 0.01, 0.05, 0.1, 0.2, 0.3, 0.4, 0.5, 0.6, 0.7, 0.8, 0.9, 0.95, 0.99, 1.0) and default settings. The "CHARMm Relative FEP Calculations (GPU)" module as implemented in Discovery Studio 2022 was used to calculate the relative free energy of binding between **21** and each new compound.

4.4. ADME prediction

To evaluate the druglikeness features of the synthesized compounds, absorption, distribution, metabolism, and excretion (ADME) predictions were performed and compared with those of compound **21** using SwissADME webserver (http://www.swissadme.ch/) [52]. Default parameters were used for ADME screening using simplified molecular input line entry system (SMILES) to import the molecular structures of the analyzed compounds. The results from SwissADME were provided through panels, each for every molecule, displaying the pharmacokinetics, physicochemical and medicinal properties of the compounds.

4.5. Synthesis

Chemicals were purchased from Sigma-Aldrich and used without further purification. Solvents were analytical grade products. Thin layer chromatography (TLC) was performed on Merck silica gel 60 F524, detected by UV-light (254 nm). Plug chromatography and column chromatography were performed on Supelco silica gel 60 Å (230−400 mesh, 40–63 μm). NMR spectra were recorded on a Bruker Avance 200 (^{1}H: 200 MHz, ^{13}C: 50 MHz) and on a Bruker Avance NEO 400 MHz (^{1}H: 400 MHz, ^{13}C: 100 MHz). DMSO-d_6 was purchased from Sigma-Aldrich, and used as received. Chemical shifts are given in ppm at room temperature and are referenced to residual protic impurities in the solvent (^{1}H: DMSO: 2.50 ppm), or to the deuterated solvent itself (^{13}C{^{1}H}: DMSO-d_6: 39.52 ppm). The resonance multiplicities are indicated as "s" (singlet), "bs" (broad singlet), "d" (doublet), and "m" (multiplet). High resolution mass spectra (HRMS) were recorded on a Xevo G2-S QTof (Waters) spectrometer, coupled with a UPLC Acquity H Class (Waters) chromatograph and on a Q Exactive Hybrid Quadrupole-Orbitrap (Thermo Fisher) spectrometer. The spectra were recorded under fast flow injection in ESI + mode, using water or methanol as eluents. Melting points were measured visually using a Stuart SMP10 melting point meter. UV–vis spectroscopy was carried out on a Varian Cary 50 Bio spectrophotometer in a quartz cuvette (edge length = 1 cm) thermostatted at 25 °C. IR spectra were taken on a Nicolet Nexus 670 spectrophotometer (resolution: 2 cm^{-1}, 20 scans). The solubility determination of compounds **21** and **1–6** was carried out in a H_2O/DMSO 99:1 mixture by the calibrated additions method. A saturated suspension of each compound was obtained by adding approximately 5 mg (excess) of each compound to 5 ml of H_2O/DMSO 99:1. Then the three suspensions were centrifuged and 1 ml of each supernatant was diluted to 100 ml with the above solvent mixture. To three aliquots (2 ml) of the solution, taken from each of the 100 ml flasks, 0.5 ml, 1.0 ml and 1.5 ml of a solution of **1–6** (**1**: 1.4 x 10^{-5} M; **2**: 2.1 x 10^{-4} M; **3**: 2.0 x 10^{-4} M; **4**: 2.3 x 10^{-4} M; **5**: 2.4 x 10^{-4} M; **6**: 2.3 x10^{-4} M in H_2O/DMSO 99:1) were added and the solutions were brought to a 5 ml volume with H_2O/DMSO 99:1, respectively. The solubility of each pyrido[2,3-*d*]pyrimidine derivative in H_2O/DMSO 99:1 was determined by plotting the intensity of the stronger absorption peak in the UV–vis spectrum (at 365 nm for **1**, at 362 nm for **2**, at 363 nm for **3**, at 361 nm for **4**, at 351 nm for **5** and at 353 nm for **6**, y-axis) against concentration (in g/ml, x-axis). The solubility is the value defined by the intercept with the x-axis of the line that passes by the three points that correspond to each sample at known concentration.

The synthesis of **21** was carried out following a previously reported literature procedure [14], and it exhibited identical spectroscopical properties to those reported. Characterizations of compounds **1–6** (NMR, HRMS, IR and UV–vis spectra) are reported in Supplementary Fig. 4-24.

Pyrido [2,3-*d*] pyrimidine-4(3*H*)-one derivative 1. Benzoylacetone (0.38 g, 2.4 mmol) and benzaldehyde (0.16 ml, 1.6 mmol) were dissolved in water (10 ml) and heated to 100 °C for 1 h. Then 2,4-diamino-6-hydroxypyrimidine (0.20 g, 1.6 mmol) was added and the

mixture was kept at 100 °C overnight. The precipitate was filtered, washed with methanol (10 ml) and purified by flash column chromatography (SiO_2, AcOEt/MeOH 95:5) to give a pale yellow powder (100 mg, 18 %). ^{1}H NMR (200 MHz, DMSO-d_6) δ (ppm): 10.32 (s, 1H, NH), 9.02 (s, 1H, NH), 7.44 (m, 5H), 7.05 (m, 5H), 6.27 (bs, 2H, NH_2), 4.91 (s, 1H, CH), 1.81 (s, 3H, CH_3). ^{13}C NMR (50 MHz, DMSO-d_6) δ (ppm): 196.68, 161.37, 154.32, 154.04, 147.26, 142.98, 141.00, 131.14, 128.41, 127.88, 127.71, 126.95, 125.67, 111.25, 90.41, 18.40. HRMS (ESI + TOF) for $C_{21}H_{18}N_4O_2$: *m/z* 359.1508 $[M+H]^+$, found: 359.1520. UV–vis (H_2O/DMSO 99:1) λ_{max} 365, 238 nm. IR (KBr pellet) $\tilde{\nu}$ = 3283, 3188, 1601, 1512, 1453, 1269 cm^{-1}. Melting point: >250 °C (dec.). Solubility (H_2O/DMSO 99:1, 25 °C): 150 μg/ml.

Pyrido [2,3-*d*] pyrimidine-4(3*H*)-one derivative 2. Benzoylacetone (0.26 g, 1.6 mmol) and 4-pyridinecarboxaldehyde (0.16 ml, 1.7 mmol) were dissolved in water (10 mL) and heated to 100 °C for 1 h. Then, 2,4-diamino-6-hydroxypyrimidine (0.20 g, 1.6 mmol) was added and the mixture was kept at 100 °C overnight. The precipitate was filtered, washed with 3 mL of methanol, and the filtrate was boiled in 10 mL of hot acetone. It was then filtered again to yield a yellowish powder, which was dried under vacuum. (380 mg, 66 %). ^{1}H NMR (200 MHz, DMSO-d_6) δ (ppm): 10.42 (s, 1H, NH), 9.19 (s, 1H, NH), 8.35 (d, J = 5.2 Hz, 2H), 7.43 (m, 5H), 7.05 (d, J = 5.2 Hz, 2H), 6.36 (bs, 2H, NH_2), 4.91 (s, 1H, CH), 1.80 (s, 3H, CH_3). ^{13}C NMR (50 MHz, DMSO-d_6) δ (ppm): 196.06, 162.35, 155.12, 154.44, 154.29, 149.31, 145.01, 141.10, 131.21, 128.50, 127.68, 122.30, 109.53, 89.26, 38.11, 18.79. HRMS (ESI + TOF) for $C_{20}H_{17}N_5O_2$: *m/z* 360.1460 $[M+H]^+$, found: 360.1522. UV–vis (H_2O/DMSO 99:1) λ_{max} 362, 281 nm. IR (KBr pellet) $\tilde{\nu}$ = 3298, 3194, 1595, 1514, 1459, 1266 cm^{-1}. Melting point: >250 °C (dec.). Solubility (H_2O/DMSO 99:1, 25 °C): 340 μg/ml.

Pyrido [2,3-*d*] pyrimidine-4(3*H*)-one derivative 3. Acetylacetone (0.30 ml, 2.9 mmol) and 4-pyridinecarboxaldehyde (0.23 ml, 2.4 mmol) were dissolved in water (10 mL) and heated to 100 °C for 1 h. Then, 2,4-diamino-6-hydroxypyrimidine (0.30 g, 2.4 mmol) was added and the mixture was reacted at 100 °C overnight. The precipitate was filtered, washed with 10 mL of water, and the filtrate was boiled in 10 mL of hot acetone. It was then filtered again to yield a yellowish powder, which was dried under vacuum. (530 mg, 74 %). ^{1}H NMR (200 MHz, DMSO-d_6) δ (ppm): 10.43 (s, 1H, NH), 9.19 (s, 1H, NH), 8.38 (d, J = 5.2 Hz, 2H), 7.20 (d, J = 5.2 Hz, 2H), 6.33 (b s, 2H, NH_2), 4.93 (s, 1H, CH), 2.35 (s, 3H, CH_3), 2.08 (s, 3H, CH_3). ^{13}C NMR (50 MHz, DMSO-d_6) δ (ppm): 195.74, 16.33, 155.26, 154.22, 153.77, 149.37, 147.91, 122.42, 109.41, 90.26, 36.54, 30.21, 19.39. HRMS (ESI + TOF) for $C_{15}H_{15}N_5O_2$: *m/z* 298.1304 $[M+H]^+$, found: 298.1294. UV–vis (H_2O/DMSO 99:1) λ_{max} 361, 280 nm. IR (KBr pellet) $\tilde{\nu}$ = 3286, 3156, 1622, 1508, 1377, 1272 cm^{-1}. Melting point: >250 °C (dec.). Solubility (H_2O/DMSO 99:1, 25 °C): 500 μg/ml.

Pyrido [2,3-*d*] pyrimidine-4(3*H*)-one derivative 4. Acetylacetone (0.60 ml, 5.9 mmol) and 3-pyridinecarboxaldehyde (0.46 ml, 4.9 mmol) were dissolved in water (20 ml) and heated to 100 °C for 1 h. Then, 2,4-diamino-6-hydroxypyrimidine (0.61 g, 4.9 mmol) was added and the mixture was reacted at 100 °C for 6 h. The precipitate was filtered, washed with 20 ml of water, and the filtrate was boiled in 10 ml of hot acetone. It was then filtered again to yield a yellowish powder, which was dried under vacuum (707 mg, 49 %). ^{1}H NMR (400 MHz, DMSO-d_6) δ (ppm): 10.39 (s, NH, 1H), 9.18 (s, NH, 1H), 8.45 (d, J = 1.8 Hz, 1H), 8.30 (dd, J = 4.7, 1.7 Hz, 1H), 7.53 (dt, J = 7.9, 2.0 Hz, 1H), 7.24 (ddd, J = 7.9, 4.8, 0.9 Hz, 1H), 6.31 (s, 2H, NH_2), 4.92 (s, 1H, CH), 2.34 (s, 3H, CH_3), 2.07 (s, 3H, CH_3). ^{13}C NMR (100 MHz, DMSO-d_6) δ (ppm): 195.87, 161.30, 154.20, 153.54, 148.63, 147.63, 146.97, 142.53, 134.56, 123.42, 109.94, 90.92, 34.91, 30.24, 19.42. HRMS (ESI + TOF) for $C_{15}H_{16}N_5O_2$: *m/z* 298.1299 $[M+H]^+$, found: 298.1292. UV–vis (H_2O/DMSO 99:1) λ_{max} 361, 287 nm. IR (KBr pellet) $\tilde{\nu}$ = 3338, 3169, 1607, 1518, 1453, 1274 cm^{-1}. Melting point: >250 °C (dec.). Solubility (H_2O/DMSO 99:1, 25 °C): 640 μg/ml.

Pyrido [2,3-*d*] pyrimidine-4(3*H*)-one derivative 5. Acetylacetone (0.60 ml, 5.9 mmol) and furfural (0.40 ml, 4.9 mmol) were dissolved in water (20 ml) and heated to 100 °C for 1 h. Then, 2,4-diamino-6-hydroxypyrimidine (0.61 g, 4.9 mmol) was added and the mixture was reacted at 100 °C for 6 h. The precipitate was filtered, washed with 20 ml of water, and the filtrate was boiled in 10 ml of hot acetone. It was then filtered again to yield a yellowish powder, which was dried under vacuum (819 mg, 59 %). ^{1}H NMR (600 MHz, DMSO-d_6) δ (ppm): 10.43 (s, 1H, NH), 9.13 (s, 1H, NH), 7.39 (dd, J = 1.8, 0.9 Hz, 1H), 6.32 (s, 2H, NH_2), 6.25 (dd, J = 3.2, 1.8 Hz, 1H), 5.87 (d, J = 3.1 Hz, 1H), 5.02 (s, 1H, CH), 2.25 (s, 3H, CH_3), 2.18 (s, 3H, CH_3). ^{13}C NMR (100 MHz, DMSO-d_6) δ (ppm): 196.13, 161.31, 158.57, 154.24, 154.20, 147.11, 141.04, 110.16, 107.84, 104.19, 88.25, 31.03, 29.68, 19.34. HRMS (ESI + TOF) for $C_{14}H_{15}N_4O_3$: *m/z* 287.1139 $[M+H]^+$, found: 287.1131. UV–vis (H_2O/DMSO 99:1) λ_{max} 351, 283 nm. IR (KBr pellet) $\tilde{\nu}$ = 3339, 3168, 1610, 1519, 1453, 1276 cm^{-1}. Melting point: >250 °C (dec.). Solubility (H_2O/DMSO 99:1, 25 °C): 500 μg/ml.

Pyrido [2,3-*d*] pyrimidine-4(3*H*)-one derivative 6. Acetylacetone (0.60 ml, 5.9 mmol) and 2-thiophenecarboxaldehyde (0.45 ml, 4.9 mmol) were dissolved in water (20 ml) and heated to 100 °C for 1 h. Then, 2,4-diamino-6-hydroxypyrimidine (0.61 g, 4.9 mmol) was added and the mixture was reacted at 100 °C for 6 h. The precipitate was filtered, washed with 20 ml of water, and the filtrate was boiled in 10 ml of hot acetone. It was then filtered again to yield a yellow powder, which was dried under vacuum (1.23 g, 84 %). ^{1}H NMR (400 MHz, DMSO-d_6) δ (ppm): 11.03 (br, 1H, NH), 9.18 (s, 1H, NH), 7.17 (dd, J = 5.1, 1.3 Hz, 1H), 6.83 (dd, J = 5.1, 3.5 Hz, 1H), 6.75 (d, J = 3.2 Hz, 1H), 5.19 (s, 1H, CH), 2.31 (s, 3H, CH_3), 2.12 (s, 3H, CH_3). ^{13}C NMR (100 MHz, DMSO-d_6) δ (ppm): 195.92, 154.70, 153.37, 152.31, 147.34, 126.45, 123.39, 122.5, 110.17, 91.37, 32.08, 29.73, 19.39. HRMS (ESI + TOF) for $C_{15}H_{15}N_5O_2$: *m/z* 303.0910 $[M+H]^+$, found: 303.0903. UV–vis (H_2O/DMSO 99:1) λ_{max} 353, 283 nm. IR (KBr pellet) $\tilde{\nu}$ = 3339, 3164, 1610, 1518, 1452, 1277 cm^{-1}. Melting point: >250 °C (dec.). Solubility (H_2O/DMSO 99:1, 25 °C): 134 μg/ml.

4.6. NEK6 kinase assays

Compounds **1–6** and **21** were dissolved in DMSO as a 10 mM stock solution and stored at −20 °C. LANCE Ultra NEK6 Kinase Assay was used to measure inhibition activity. Briefly, the compounds were tested at 30 μM by incubation with 4 nM NEK6 (Carna, Chuo-ku, Kobe, Japan, # 05–130), 50 nM ULight-p70 S6K Peptide (PerkinElmer # TRF0126) and 100 μM ATP (Sigma-Aldrich, Saint Louis, U.S.A, #A2383) at room temperature, as previously reported [9]. We note that the inhibition activity studies were carried out on compounds **1–6** as racemic mixtures, in line with what was done earlier for compound **21** [9]. After 90 min, the kinase reaction was stopped by adding 40 mM EDTA and then the detection mix, composed of 2 nM Eu-*anti*-phospho-p70 S6K antibody, was added. The read signal has been detected with the Enspire multimode plate reader (PerkinElmer) in TR-FRET mode (excitation at 320 nm and emission at 665 nm) after 60 min. Inhibition of NEK6 activity was calculated as a percentage of the control sample (100 % of activity).

4.7. SAR/QSAR analysis

A set of 94 easily interpretable molecular descriptors (MoDs) were initially calculated by the Dragon software (v.6.0) [44] for compounds 21 and 1–6, which included descriptors of the following typology: constitutional indices, ring features, geometrical descriptors, functional group counts, charge descriptors, molecular properties and drug-like indices. MoDs were filtered to exclude those with two or fewer unique values and those with a range equal to or below 10 % of their maximum value. The retained 37 MoDs were taken for our SAR study and an autocorrelation analysis was first carried out to discard multicollinearity (CSV files with the filtered MoDs dataset and the autocorrelation matrix are provided as **Supplementary files**). Supplementary Fig. 27 depicts a heatmap based on the obtained autocorrelation matrix. MoDs were scaled to avoid scaling issues. Ordinary Least Squares (OLS) multiple

linear regression method (MLR) was employed to evaluate the potential SARs in our dataset in relation to the endpoint measurements obtained along this work: NEK6 % inhibition (Fig. 5) and compounds' solubility (Supplementary Table 3). The statistical parameter squared Pearson correlation coefficient (R^2) was used to assess the SAR's relevance. Individual SARs were obtained for each MoD (see Supplementary Table 4). *Ad-hoc* Python scripts were prepared to perform all regression and autocorrelation analyses. The leave-one-out cross-validation coefficient (loo-q2) –typically used to assess the internal predictability of regression models– was not considered here due to the small dataset available for this study. Likewise, no test or external sets were established for validation due to the same reason.

CRediT authorship contribution statement

Paolo Zardi: Writing – review & editing, Formal analysis, Conceptualization. **Benedetta Righino:** Writing – review & editing, Investigation, Formal analysis, Conceptualization. **Davide Pirolli:** Writing – review & editing, Investigation, Formal analysis, Conceptualization. **Matteo Gramanzini:** Writing – review & editing, Investigation, Formal analysis. **Alessandro Semeraro:** Writing – review & editing, Investigation. **Juan José Galano-Frutos:** Writing – review & editing, Investigation, Formal analysis. **Anna Königs:** Writing – review & editing, Investigation. **Luka Đorđević:** Writing – review & editing. **Michele Maggini:** Writing – review & editing, Writing – original draft, Conceptualization. **Marianna Buttarelli:** Writing – review & editing, Formal analysis. **Natalia Cappoli:** Writing – review & editing, Investigation, Formal analysis. **Viviana Romano:** Writing – review & editing, Investigation. **Marta De Donato:** Writing – review & editing, Investigation, Formal analysis. **Daniela Gallo:** Writing – review & editing. **Giovanni Scambia:** Writing – review & editing. **Maria Cristina De Rosa:** Writing – review & editing, Writing – original draft, Conceptualization.

Declaration of interests

The authors declare that they have no known competing financial interests or personal relationships that could have appeared to influence the work reported in this paper.

Acknowledgements

We thank E. Marotta for her help in the HR-MS analysis; T. Carofiglio, A. Pavan and M. Ranotto for solubility measurements and syntheses optimization and A. Basagni for TEM characterization.

Appendix. A Supplementary data

Supplementary data to this article can be found online at https://doi.org/10.1016/j.abb.2025.110391.

Data availability

Data will be made available on request.

References

[1] M.-J. Yin, L. Shao, D. Voehringer, T. Smeal, B. Jallal, The serine/threonine kinase Nek6 is required for cell cycle progression through mitosis, J. Biol. Chem. 278 (2003) 52454–52460, https://doi.org/10.1074/jbc.M308080200.
[2] Z. He, X. Ni, L. Xia, Z. Shao, Overexpression of NIMA-related kinase 6 (NEK6) contributes to malignant growth and dismal prognosis in Human Breast Cancer, Pathol. Res. Pract. 214 (2018) 1648–1654, https://doi.org/10.1016/j.prp.2018.07.030.
[3] E. Kasap, E. Gerceker, S.Ö. Boyacıoglu, H. Yuceyar, H. Yıldırm, S. Ayhan, M. Korkmaz, The potential role of the NEK6, AURKA, AURKB, and PAK1 genes in adenomatous colorectal polyps and colorectal adenocarcinoma, Tumor Biol. 37 (2016) 3071–3080, https://doi.org/10.1007/s13277-015-4131-6.
[4] B. Zhang, H. Zhang, D. Wang, S. Han, K. Wang, A. Yao, X. Li, Never in mitosis gene A-related kinase 6 promotes cell proliferation of hepatocellular carcinoma via cyclin B modulation, Oncol. Lett. 8 (2014) 1163–1168, https://doi.org/10.3892/ol.2014.2300.
[5] M.D. Donato, M. Fanelli, M. Mariani, G. Raspaglio, D. Pandya, S. He, P. Fiedler, M. Petrillo, G. Scambia, C. Ferlini, Nek6 and Hif-1α cooperate with the cytoskeletal gateway of drug resistance to drive outcome in serous ovarian cancer, Am. J. Cancer Res. 5 (2015) 1862–1877.
[6] N.K. Panchal, S. Mohanty, S.E. Prince, NIMA-related kinase-6 (NEK6) as an executable target in cancer, Clin. Transl. Oncol. 25 (2022) 66–77, https://doi.org/10.1007/s12094-022-02926-4.
[7] P. Srinivasan, P. Chella Perumal, A. Sudha, Discovery of novel inhibitors for Nek6 protein through homology model assisted structure based virtual screening and molecular docking approaches, Sci. World J. 2014 (2014), https://doi.org/10.1155/2014/967873.
[8] E. Moraes, G. Meirelles, R. Honorato, T. De Souza, E. De Souza, M. Murakami, P. De Oliveira, J. Kobarg, Kinase inhibitor profile for human Nek1, Nek6, and Nek7 and analysis of the structural basis for inhibitor specificity, Molecules 20 (2015) 1176–1191, https://doi.org/10.3390/molecules20011176.
[9] M. De Donato, B. Righino, F. Filippetti, A. Battaglia, M. Petrillo, D. Pirolli, G. Scambia, M.C. De Rosa, D. Gallo, Identification and antitumor activity of a novel inhibitor of the NIMA-related kinase NEK6, Sci. Rep. 8 (2018) 16047, https://doi.org/10.1038/s41598-018-34471-y.
[10] De Rosa, Maria Cristina, Davide Pirolli, Giovanni Scambia, Daniela Gallo, Marco Petrillo, Marta De Donato, Righino Benedetta, NEK6 Kinase Inhibitors Useful for the Treatment of Solid Tumors, 2019. WO2019193494A1.
[11] B. Das, A.T.K. Baidya, A.T. Mathew, A.K. Yadav, R. Kumar, Structural modification aimed for improving solubility of lead compounds in early phase drug discovery, Bioorg. Med. Chem. 56 (2022) 116614, https://doi.org/10.1016/j.bmc.2022.116614.
[12] K.U. Khan, M.U. Minhas, S.F. Badshah, M. Suhail, A. Ahmad, S. Ijaz, Overview of nanoparticulate strategies for solubility enhancement of poorly soluble drugs, Life Sci. 291 (2022) 120301, https://doi.org/10.1016/j.lfs.2022.120301.
[13] M. Ishikawa, Y. Hashimoto, Improvement in aqueous solubility in small molecule drug discovery programs by disruption of molecular planarity and symmetry, J. Med. Chem. 54 (2011) 1539–1554, https://doi.org/10.1021/jm101356p.
[14] S. Tu, Y. Zhang, H. Jiang, B. Jiang, J. Zhang, R. Jia, F. Shi, A simple synthesis of furo[3′,4′:5,6]pyrido[2,3- *d*]pyrimidine derivatives through multicomponent reactions in water, Eur. J. Org Chem. 2007 (2007) 1522–1528, https://doi.org/10.1002/ejoc.200600913.
[15] V.E. Saraev, I.M. Zviagin, R.G. Melik-Oganjanyan, Y.V. Sen'ko, S.M. Desenko, V. A. Chebanov, Green microwave-assisted multicomponent route to the formation of 5,8-dihydropyrido[2,3- *d*]pyrimidine skeleton in aqueous media, J. Heterocycl. Chem. 54 (2017) 318–324, https://doi.org/10.1002/jhet.2586.
[16] J.M. Jumper, Richard O. Evans, R. Evans, R.F.L. Evans, A. Pritzel, T. Green, M. Figurnov, O. Ronneberger, K. Tunyasuvunakool, R. Bates, Russ Bates, Russ Bates, A. Žídek, A. Potapenko, Anna Potapenko, A. Bridgland, C. Meyer, S.A. A. Kohl, A.J. Ballard, Andrew Cowie, Andrew Cowie, A.M. Cowie, B. Romera-Paredes, S. Nikolov, Rishub Jain, R.D. Jain, J. Adler, Jonas Adler, T. Back, S. Petersen, D. Reiman, E. Clancy, M. Zielinski, J. Söding, M. Steinegger, M. Pacholska, M. Pacholska, T. Berghammer, Sebastian Bodenstein, Sebastian Bodenstein, D. Silver, D.L. Silver, D. Silver, O. Vinyals, A.W. Senior, K. Kavukcuoglu, P. Kohli, D. Hassabis, Highly accurate protein structure prediction with AlphaFold, Nature 596 (2021) 583–589, https://doi.org/10.1038/s41586-021-03819-2.
[17] M. Varadi, S. Anyango, M. Deshpande, S. Nair, Cindy Natassia, G. Yordanova, D. Y. Yuan, O. Stroe, Gemma Wood, A. Laydon, A. Žídek, T.R. Green, T. Green, K. Tunyasuvunakool, S. Petersen, J.M. Jumper, E. Clancy, R.E. Green, Ankur Vora, Mira Lutfi, M. Figurnov, A.M. Cowie, Andrew Cowie, Nicole Hobbs, P. Kohli, G. J. Kleywegt, E. Birney, D. Hassabis, S. Velankar, AlphaFold Protein Structure Database: massively expanding the structural coverage of protein-sequence space with high-accuracy models, Nucleic Acids Res. (2021), https://doi.org/10.1093/nar/gkab1061.
[18] I. Westwood, D.-M. Cheary, J.E. Baxter, M.W. Richards, R.L.M. van Montfort, A. M. Fry, R. Bayliss, Insights into the conformational variability and regulation of human Nek2 kinase, J. Mol. Biol. 386 (2009) 476–485, https://doi.org/10.1016/j.jmb.2008.12.033.
[19] X. Zhang, J. Gureasko, K. Shen, P.A. Cole, J. Kuriyan, An allosteric mechanism for activation of the kinase domain of epidermal growth factor receptor, Cell 125 (2006) 1137–1149, https://doi.org/10.1016/j.cell.2006.05.013.
[20] F. Sicheri, J. Kuriyan, Structures of Src-family tyrosine kinases, Curr. Opin. Struct. Biol. 7 (1997) 777–785, https://doi.org/10.1016/S0959-440X(97)80146-7.
[21] G.V. Meirelles, J.C. Silva, Y. de A. Mendonça, C.H. Ramos, I.L. Torriani, J. Kobarg, Human Nek6 is a monomeric mostly globular kinase with an unfolded short N-terminal domain, BMC Struct. Biol. 11 (2011) 12, https://doi.org/10.1186/1472-6807-11-12.
[22] A. Zerroug, S. Belaidi, I. BenBrahim, L. Sinha, S. Chtita, Virtual screening in drug-likeness and structure/activity relationship of pyridazine derivatives as Anti-Alzheimer drugs, J. King Saud Univ. Sci. 31 (2019) 595–601, https://doi.org/10.1016/j.jksus.2018.03.024.
[23] C.A. Lipinski, Drug-like properties and the causes of poor solubility and poor permeability, J. Pharmacol. Toxicol. Methods 44 (2000) 235–249, https://doi.org/10.1016/S1056-8719(00)00107-6.
[24] N.A. Meanwell, Improving drug candidates by design: a focus on physicochemical properties as a means of improving compound disposition and safety, Chem. Res. Toxicol. 24 (2011) 1420–1456, https://doi.org/10.1021/tx200211v.
[25] R.D. Hernandez, F.A.F. Genio, J.R. Casanova, M.T. Conato, M.C. Paderes, Antiproliferative activities and SwissADME predictions of physicochemical

properties of carbonyl group-modified rotenone analogues, Chem.Open (2023) e202300087, https://doi.org/10.1002/open.202300087.
[26] C.A. Lipinski, Lead- and drug-like compounds: the rule-of-five revolution, Drug Discov. Today Technol. 1 (2004) 337–341, https://doi.org/10.1016/j.ddtec.2004.11.007.
[27] T.T. Wager, X. Hou, P.R. Verhoest, A. Villalobos, Central nervous system multiparameter optimization desirability: application in drug discovery, ACS Chem. Neurosci. 7 (2016) 767–775, https://doi.org/10.1021/acschemneuro.6b00029.
[28] J.D. Hughes, J. Blagg, D.A. Price, S. Bailey, G.A. DeCrescenzo, R.V. Devraj, E. Ellsworth, Y.M. Fobian, M.E. Gibbs, R.W. Gilles, N. Greene, E. Huang, T. Krieger-Burke, J. Loesel, T. Wager, L. Whiteley, Y. Zhang, Physiochemical drug properties associated with in vivo toxicological outcomes, Bioorg. Med. Chem. Lett 18 (2008) 4872–4875, https://doi.org/10.1016/j.bmcl.2008.07.071.
[29] A. Daina, V. Zoete, A BOILED-egg to predict gastrointestinal absorption and brain penetration of small molecules, ChemMedChem 11 (2016) 1117–1121, https://doi.org/10.1002/cmdc.201600182.
[30] R.B. Kim, Drugs as P-glycoprotein substrates, inhibitors, and inducers, Drug Metab. Rev. 34 (2002) 47–54, https://doi.org/10.1081/DMR-120001389.
[31] D.F. Veber, S.R. Johnson, H.-Y. Cheng, B.R. Smith, K.W. Ward, K.D. Kopple, Molecular properties that influence the oral bioavailability of drug candidates, J. Med. Chem. 45 (2002) 2615–2623, https://doi.org/10.1021/jm020017n.
[32] Y.C. Martin, A bioavailability score, J. Med. Chem. 48 (2005) 3164–3170, https://doi.org/10.1021/jm0492002.
[33] J.B. Baell, J.W.M. Nissink, Seven year itch: pan-assay interference compounds (PAINS) in 2017—utility and limitations, ACS Chem. Biol. 13 (2018) 36–44, https://doi.org/10.1021/acschembio.7b00903.
[34] D. Shi, L. Niu, H. Yao, H. Jiang, An efficient synthesis of pyrimido[4,5- *b*]quinoline derivatives *via* three-component reaction in aqueous media, J. Heterocycl. Chem. 46 (2009) 237–242, https://doi.org/10.1002/jhet.57.
[35] Y. Yang, M. Gao, W.-M. Shu, L.-M. Wu, D.-X. Zhang, A.-X. Wu, Synthesis of α-iodoketals from methyl ketones via sustainable and orthogonal tandem catalysis, Org. Biomol. Chem. 11 (2013) 1226, https://doi.org/10.1039/c2ob27028e.
[36] J. Chang, C. Xu, J. Gao, F. Gao, D. Zhu, M. Wang, Me $_3$ SiCF $_2$ Br-Self-Assisted domino reaction: catalytic synthesis of α,α-difluorocyclopentanones from methylvinylketones, Org. Lett. 19 (2017) 1850–1853, https://doi.org/10.1021/acs.orglett.7b00611.
[37] R.-G. Xing, Y.-N. Li, Q. Liu, Y.-F. Han, X. Wei, J. Li, B. Zhou, Selective reduction of nitroarenes by a hantzsch 1,4-dihydropyridine: a facile and efficient approach to substituted quinolines, Synthesis (2011) 2066–2072, https://doi.org/10.1055/s-0030-1260609 (2011).
[38] T. Allam, D.E. Balderston, M.K. Chahal, K.L.F. Hilton, C.K. Hind, O.B. Keers, R. J. Lilley, C. Manwani, A. Overton, P.I.A. Popoola, L.R. Thompson, L.J. White, J. R. Hiscock, Tools to enable the study and translation of supramolecular amphiphiles, Chem. Soc. Rev. 52 (2023) 6892–6917, https://doi.org/10.1039/D3CS00480E.
[39] R. Todeschini, V. Consonni, Handbook of Molecular Descriptors, first ed., Wiley, 2000 https://doi.org/10.1002/9783527613106.
[40] U.P. P, M. Suresh, F.T. Tolasa, E. Bonyah, QSPR/QSAR study of antiviral drugs modeled as multigraphs by using TI's and MLR method to treat COVID-19 disease, Sci. Rep. 14 (2024) 13150, https://doi.org/10.1038/s41598-024-63007-w.
[41] L.K. Tsou, S.-H. Yeh, S.-H. Ueng, C.-P. Chang, J.-S. Song, M.-H. Wu, H.-F. Chang, S.-R. Chen, C. Shih, C.-T. Chen, Y.-Y. Ke, Comparative study between deep learning and QSAR classifications for TNBC inhibitors and novel GPCR agonist discovery, Sci. Rep. 10 (2020) 16771, https://doi.org/10.1038/s41598-020-73681-1.
[42] J.J.G. Javier Sancho, QSAR models for prediction of binding and inhibitory properties of [(E)-2- R-vinyl]benzene derivatives with therapeutic effects against Helicobacter pylori, Med. Chem. 4 (2013), https://doi.org/10.4172/2161-0444.1000157.
[43] Gustavo A. Arteca, Molecular shape descriptors, Reviews in Computational Chemistry, 1991, pp. 191–253, https://doi.org/10.1002/9780470125861.ch5.
[44] D.A. Belsley, E. Kuh, R.E. Welsch, Regression Diagnostics: Identifying Influential Data and Sources of Collinearity, Wiley, New York, 2005, https://doi.org/10.1002/0471725153.
[45] C. Colovos, T.O. Yeates, Verification of protein structures: patterns of nonbonded atomic interactions, Protein Sci. 2 (1993) 1511–1519, https://doi.org/10.1002/pro.5560020916.
[46] R.A. Laskowski, M.W. MacArthur, D.S. Moss, J.M. Thornton, PROCHECK: a program to check the stereochemical quality of protein structures, J. Appl. Crystallogr. 26 (1993) 283–291, https://doi.org/10.1107/S0021889892009944.
[47] M. Wiederstein, M.J. Sippl, ProSA-web: interactive web service for the recognition of errors in three-dimensional structures of proteins, Nucleic Acids Res. 35 (2007) W407–W410, https://doi.org/10.1093/nar/gkm290.
[48] C.J. Williams, J.J. Headd, N.W. Moriarty, M.G. Prisant, L.L. Videau, L.N. Deis, V. Verma, D.A. Keedy, B.J. Hintze, V.B. Chen, S. Jain, S.M. Lewis, W.B. Arendall, J. Snoeyink, P.D. Adams, S.C. Lovell, J.S. Richardson, D.C. Richardson, MolProbity: more and better reference data for improved all-atom structure validation, Protein Sci. 27 (2018) 293–315, https://doi.org/10.1002/pro.3330.
[49] C. Lu, C. Wu, D. Ghoreishi, W. Chen, L. Wang, W. Damm, G.A. Ross, M.K. Dahlgren, E. Russell, C.D. Von Bargen, R. Abel, R.A. Friesner, E.D. Harder, OPLS4: improving force field accuracy on challenging regimes of chemical space, J. Chem. Theor. Comput. 17 (2021) 4291–4300, https://doi.org/10.1021/acs.jctc.1c00302.
[50] T. Darden, D. York, L. Pedersen, Particle mesh Ewald: an $N \cdot \log(N)$ method for Ewald sums in large systems, J. Chem. Phys. 98 (1993) 10089–10092, https://doi.org/10.1063/1.464397.
[51] G.J. Martyna, D.J. Tobias, M.L. Klein, Constant pressure molecular dynamics algorithms, J. Chem. Phys. 101 (1994) 4177–4189, https://doi.org/10.1063/1.467468.
[52] A. Daina, O. Michielin, V. Zoete, SwissADME: a free web tool to evaluate pharmacokinetics, drug-likeness and medicinal chemistry friendliness of small molecules, Sci. Rep. 7 (2017) 42717, https://doi.org/10.1038/srep42717.